



RESEARCH ARTICLE

# Pre-instrumental summer precipitation variability in northwestern Greece from a high-elevation *Pinus heldreichii* network

Jan Esper<sup>1</sup>  | Oliver Konter<sup>1</sup> | Lara Klippel<sup>2</sup>  | Paul J. Krusic<sup>3</sup> | Ulf Büntgen<sup>3,4,5</sup>

<sup>1</sup>Department of Geography, Johannes Gutenberg University, Mainz, Germany

<sup>2</sup>Department of Geography, Justus Liebig University, Giessen, Germany

<sup>3</sup>Department of Geography, University of Cambridge, Cambridge, UK

<sup>4</sup>Swiss Federal Research Institute WSL, Birmensdorf, Switzerland

<sup>5</sup>Global Change Research Centre AS CR v. v.i, Brno, Czech Republic

## Correspondence

Jan Esper, Department of Geography, Johannes Gutenberg University, Mainz, Germany.

Email: [esper@uni-mainz.de](mailto:esper@uni-mainz.de)

## Funding information

Deutsche Forschungsgemeinschaft, Grant/Award Number: ES 161/12-1

## Abstract

The spatiotemporal variability of precipitation is of vital importance to Mediterranean ecology and economy, but pre-instrumental changes are not well understood. Here, we present a millennial-length June–July precipitation reconstruction derived from a network of 22 *Pinus heldreichii* high-elevation sites in the Pindus Mountains of northwestern Greece. Tree-ring width chronologies from these sites cohere exceptionally well over the past several hundred years ( $r_{1467-2015} = 0.64$ ) revealing coherence at inter-annual to centennial timescales across the network. The network mean calibrates significantly against instrumental June–July precipitation over the past 40 years ( $r_{1976-2015} = 0.71$ ), even though no high-elevation observational record is available representing the moist conditions at the treeline above 1,900 m a.s.l. For the final reconstruction, the instrumental target data are adjusted to provide realistic estimates of high-elevation summer rainfall back to 729 CE. The reconstruction contains substantially more low-frequency variability than other high-resolution hydroclimate records from the eastern Mediterranean including extended dry periods from 1,350 to 1,379 CE ( $39 \pm 4.5$  mm) and 913 to 942 ( $40 \pm 8.4$  mm), and moist periods from 862 to 891 ( $86 \pm 11$  mm) and 1,522 to 1,551 ( $80 \pm 3.5$  mm), relative to the long-term mean of 61 mm. The most recent 30-year period from 1986 to 2015 is characterized by above average June–July precipitation ( $73 \pm 2$  mm). Low-frequency changes in summer precipitation are likely related to variations in the position and persistence of storm tracks steering local depressions and causing extensive rainfall (or lack thereof) in high-elevation environments of the Pindus Mountains.

## KEYWORDS

climate reconstruction, Mediterranean, Pindus Mountains, pine, tree-rings, Valia Calda

## 1 | INTRODUCTION

The Pindus Mountains in northwestern Greece are an important source of irrigation water supplying lowland agricultural systems during the dry Mediterranean summer periods. The mountain range is located in a relatively moist belt in northern Greece extending from the Albanian border in the west to the Thracian Sea in the east, where (low elevation) meteorological stations record between 30 and 40 mm precipitation from June to July (Figure 1). These values are, however, not representative of the high-elevation environments of the Pindus Mountains, including the Valia Calda in the Pindus National Park (PNP) and the second highest peak in Greece, the Mt. Smolikas massif at 2,637 m a.s.l. (insert diagrams in Figure 1), where rain-laden thunderstorms frequently occur during summertime and annual precipitation is estimated to exceed 1,600 mm (Fotiadi *et al.*, 1999). Several high-elevation PNP areas >1,900 m a.s.l. are covered by steppe-like forests including giant Bosnian pines (*Pinus heldreichii*) reaching ages >1,000 years (Konter *et al.*, 2017). These trees provide a unique opportunity to reconstruct regional hydroclimatic variability over the past millennium and place the recent, anthropogenically changed dynamics in a long-term context.

Associated with a strengthening of circum-global subtropical high-pressure belts, climate models unequivocally predict a decrease of Mediterranean precipitation, accompanied by an increase of (dry and moist) extreme events in the upcoming decades (Li *et al.*, 2012). Long-term desiccation will amplify evaporative demand

challenging plant metabolism and foster an even greater need to irrigate Mediterranean crops (Zhang and Oweis, 1999). Several high-resolution hydroclimate reconstructions extending over the past 500+ years have been developed in the eastern Mediterranean to place these impending dynamics into historical perspective. These include a 900-year reconstruction of May–June precipitation from oak tree-ring widths (TRW) in northern Greece and northeastern Turkey (Griggs *et al.*, 2007) and a 600-year May–August precipitation reconstruction from trees in Turkey, Syria, Lebanon, Cyprus, and Greece (Touchan *et al.*, 2005). Both these records have been constructed in a manner that emphasizes high-frequency, inter-annual precipitation variability over the past centuries and are therefore of limited value to assess lower-frequency hydroclimatic changes at longer timescales. Similarly, a June–July standardized precipitation index (SPI) reconstruction extending back to eighth century CE has been produced using Mt. Smolikas *Pinus heldreichii* TRW data (Klippel *et al.*, 2018) but due to the challenges of accurately modelling decadal to multi-decadal variability in TRW data that contain persistent ontogenetic trends (Esper *et al.*, 2015b), this record is also constrained to represent just the high-frequency variance in precipitation. TRW data from several sites in the eastern Mediterranean have also been integrated in a European drought atlas, providing spatially resolved reconstructions of the June–August Palmer Drought Severity Index (PDSI) over the past millennium (Cook *et al.*, 2015). Compared to the precipitation and SPI reconstructions (Touchan *et al.*, 2005; Griggs *et al.*, 2007; Klippel *et al.*, 2018), the

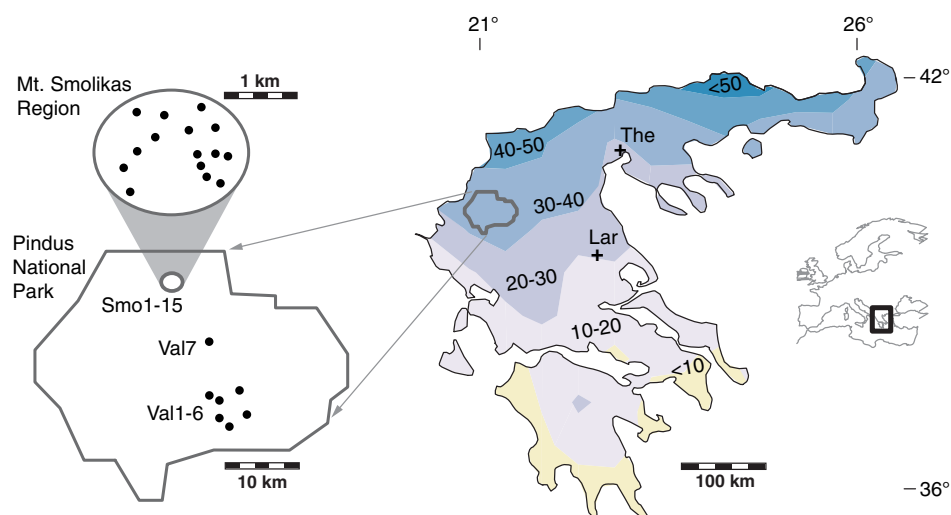


**FIGURE 1** Map showing the south-to-north precipitation gradient in Greece, the Pindus National Park (PNP) in northwestern Greece (bottom left), and the Mt. Smolikas region (top left). Black dots mark the high-elevation *Pinus heldreichii* network (HEPI) including the Val1-7 and Smo1-15 tree-ring sampling sites. Black crosses indicate the location of major cities Larissa (Lar) and Thessaloniki (The) hosting long instrumental precipitation stations reaching back to 1951 and 1931, respectively. Contour colours and values refer to average June–July precipitation in mm per year from 1976 to 2015 [Colour figure can be viewed at [wileyonlinelibrary.com](https://onlinelibrary.wiley.com)]

reconstructed PDSI from those grid points centred over the PNP region in northwestern Greece contain more low-frequency variance. This is likely due to the fact that both precipitation and temperature variability are incorporated in this drought index (van der Schrier *et al.*, 2013). An unprecedented trend towards lower PDSI values since the late 20th century (Cook *et al.*, 2015) is likely driven by rising temperatures since instrumental precipitation data display no recent decline (Hatzianastassiou *et al.*, 2008; Harris *et al.*, 2014).

Here, we place the recent hydroclimate dynamics into a long-term context and explore the feasibility of reconstructing low-frequency, inter-decadal to centennial precipitation variability by employing a network of 22 high-elevation *Pinus heldreichii* (HEPI) site chronologies from northwestern Greece. A variety of detrending methods are applied to this network to remove ontogenetic trends from TRW data and assess the covariance among HEPI site chronologies over the past several centuries. We produce a network mean integrating all HEPI TRW data, calibrate this timeseries against instrumental precipitation data, and reconstruct high-to-low frequency June–July precipitation variability back to 729 CE. Finally, the HEPI reconstruction is compared with existing records to assess and discuss long-term hydroclimatic changes in the eastern Mediterranean and their potential underlying forcings.

## 2 | DATA AND METHODS

### 2.1 | High-elevation *Pinus heldreichii* network

Between 2015 and 2019, we conducted five field campaigns to establish the HEPI network. The network includes TRW chronologies from 22 PNP *Pinus heldreichii* sites above 1,900 m a.s.l., 15 of which are located within ~2 km on the Mt. Smolikas massif (Smo1–15 hereafter) and seven are distributed over Valia Calda (Val1–7; Figure 1 and Figure S1, Table S1). All sampling sites are located near the upper treeline, characterized by a steppe-like vegetation including large solitary Bosnian pines (Klippel *et al.*, 2017, 2019; Konter *et al.*, 2017). Ground surfaces are characterized by a heterogeneous mosaic of shallow-to-deep cambic fluvisols and partially mobile rock fields over serpentinite bedrock, in which *Pinus heldreichii* is the only dominant tree species accompanied by a shallow-to-inexistent understory of various true and obligate serpentinophyte shrubs and grasses. Fairly unique to Mediterranean forests, several HEPI sites are littered with dead stem sections, sun-bleached relic portions of trees that once lived, and have remained for centuries on crumbling rock fields overlying the soils. The

combination of TRW data from these relict samples with measurements from living trees enabled us to develop several composite chronologies extending back into the first millennium of the Common Era (Figure 2).

The HEPI network includes 1,136 TRW series representing 591 individual trees. Among the 22 sites replication varies significantly, from 12 to 158 radii. This skewed distribution is a consequence of investing more sampling effort in the very old sites (Table 1). The pines are on average quite old (316 years) and produce relatively narrow rings (0.86 mm). The average interseries correlation ( $R_{bar}$ ; Cook and Kairiukstis, 1990; Fritts, 2012) across the whole network is 0.28, and ranges from 0.24 in Smo13 to 0.42 in Smo4 and 15, all of which are towards the lower end of coherency values reported from other millennial-length tree-ring compilations worldwide (Esper *et al.*, 2016; Ljungqvist *et al.*, 2020). The  $R_{bar}$  values appear to be independent of site exposure and elevation (Table S1).

### 2.2 | Detrending, calibration and reconstruction methods

The 1,136 TRW series were detrended by calculating residuals from 50-, 100-, 300- and 500-year splines to emphasize different frequencies in the resulting chronologies (Cook and Peters, 1981). Prior to detrending, the series were power transformed to minimize curve fitting end-effects that can arise with stiff (300- and 500-year) splines applied to slow growing trees (Cook and Peters, 1997). The detrended series were averaged using a bi-weight robust mean to produce 22 site chronologies as well as a HEPI mean chronology integrating >350,000 tree rings from all 591 trees. To account for effects of changing replication and covariance through time (Osborn *et al.*, 1997; Frank *et al.*, 2007), the mean timeseries were variance-stabilized by calculating ratios from 300-year splines fitted to the absolute values of annual departures from the chronology means using the latest Arstan software (49v1a opt. 13; Meko *et al.*, 1993; Cook *et al.*, 2017). The individual site chronologies were truncated to the year when their respective minimum replication falls below five TRW series (radii), and the HEPI chronology was truncated in 729 CE when replication falls below 20 TRW series.

Network covariance was assessed by calculating correlations among the 500-year spline detrended sites chronologies (from 1467 to 2015), as well as between the regional mean chronologies integrating the 15 Smo sites and 7 Val sites (from 1227 to 2015). Site and HEPI mean chronologies were calibrated against regional precipitation and temperature data extracted from grid points between 39°–40°N and 21°–24°E in the CRU TS 4.04 dataset (Harris *et al.*, 2014). This was done over different

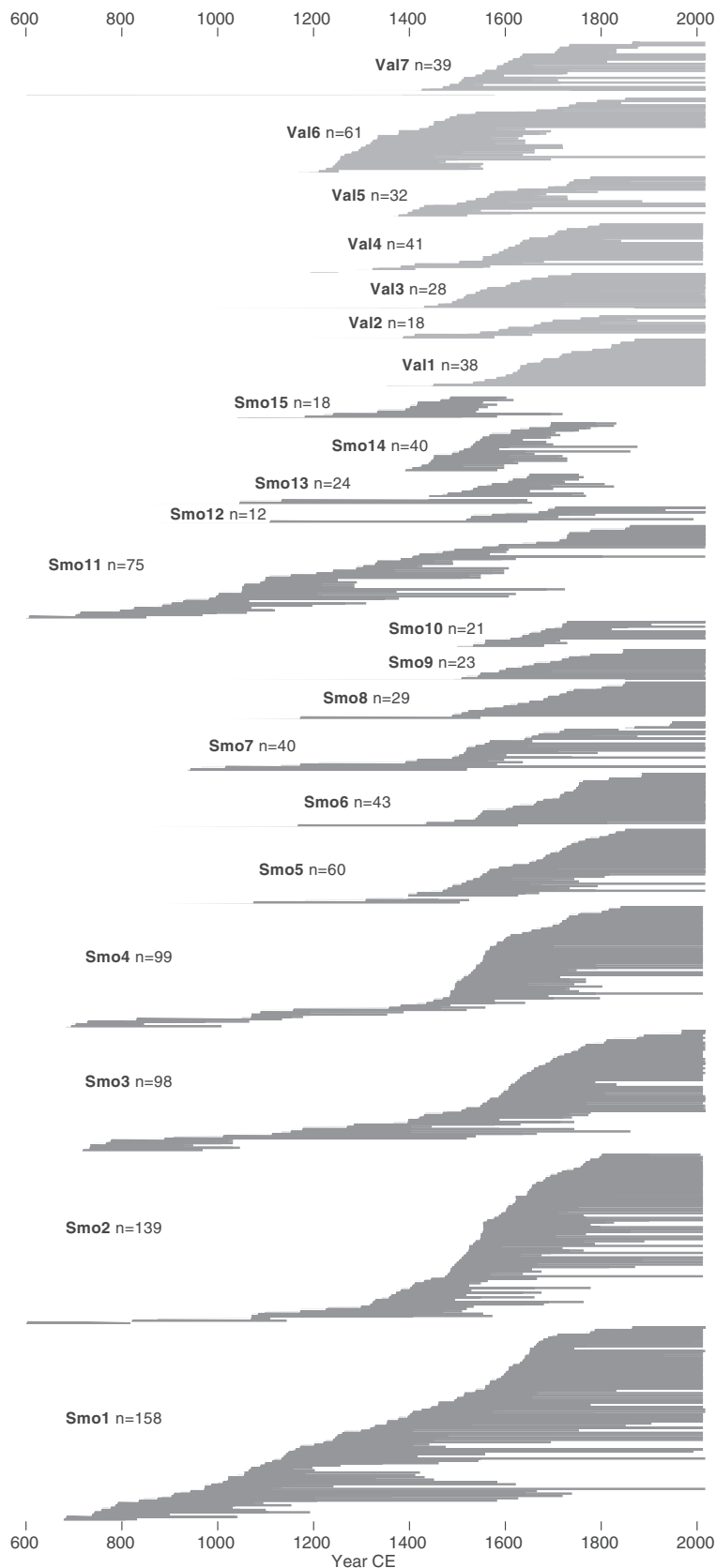


**FIGURE 2** Bar plot showing the sample replication of sites Val1-7 (top) and Smo1-15 of the high-elevation *Pinus heldreichii* network since 600 CE. Each horizontal bar represents one measured TRW radius

periods, 1901–2015, 1951–2015, 1961–2015 and 1976–2015, in recognition of the declining numbers of instrumental stations back in time (Klippel *et al.*, 2018).

Climate-growth assessments were performed using monthly and mean June–July precipitation totals, and spatial correlation patterns assessed using KNMI's

**TABLE 1** Characteristics of the high-elevation *Pinus heldreichii* network including 22 sites between 1,900 and 2,210 m a.s.l. in the Pindus Mountains

	Per site	Network
Number of trees	8–81	591
Number of radii	12–158	1,136
Mean segment length (yrs)	167–428	316
Average growth rate (mm)	0.61–1.24	0.86
Interseries correlation (Rbar)	0.24–0.42	0.28
Inter-site correlation <sup>a</sup>	0.64	–
June–July precip. corr. <sup>b</sup>	0.26–0.76	0.71

<sup>a</sup>From 1476 to –2015. Period not fully covered by all sites.

<sup>b</sup>From 1976 to 2015 against CRU TS 4.04.

climate explorer (Trouet and Van Oldenborgh, 2013). As the CRU TS 4.04 average precipitation during June and July (23 mm) does not represent the moist conditions at the PNP treeline environments, the monthly data were adjusted by adding another 50 mm before producing final reconstructions. This was done to rescale the CRU TS 4.04 interpolated grid point values with the much wetter summer and annual estimates reported from regional studies (Fotiadi *et al.*, 1999) and avoid calculating meaningless negative reconstructed precipitation values over the past millennium.

The HEPI mean chronology was regressed (Esper *et al.*, 2005) against adjusted June–July precipitation data from 1976 to 2015 to produce a formal reconstruction of PNP high-elevation rainfall over the past 1,278 years. Reconstruction uncertainty was estimated by calculating 95% bootstrap confidence intervals derived from resampling and averaging the detrended TRW data with replacement 1,000 times (Briffa *et al.*, 1992). Moving interseries correlations (Rbar; Fritts, 1976) and expressed population signal timeseries (EPS; Wigley *et al.*, 1984) were computed over 50-year intervals, shifted in 25-year steps, to evaluate temporal changes in data coherency back to 729 CE. Potential shifts in signal strength were analysed by splitting the instrumental data into two equally long calibration and verification sequences (1976–1995, 1996–2015) and calculating the reduction of error (RE) and coefficient of efficiency (CE) statistics to estimate the skill of modelled precipitation compared to the instrumental means of the calibration and verification periods (Cook *et al.*, 1994). The Durbin–Watson statistic (DW) was calculated to quantify autocorrelation in the residuals between the modelled and measured precipitation data (Durbin and Watson, 1951). Whereas positive RE and CE values indicate some statistical skill of the reconstruction, DW values above 1 point to minor drifts between the predictand and predictor.

## 3 | RESULTS AND DISCUSSION

### 3.1 | TRW coherency and climate signals

Growth coherence is exceptionally high across the HEPI network as indicated by an inter-site correlation of  $r = 0.64$  from 1476 to 2015 (Table 1). This coherency is reflected in both high-frequency extremes and lower-frequency trends that are closely aligned among the Smo and Val site chronologies (Figure 3). The Smo and Val mean timeseries (shown in red in Figure 3) correlate at  $r = 0.77$  over the past eight centuries suggesting that some climatic forcing synchronized TRW variability across the PNP. This correlation declines from  $r = 0.83$  since 1,501 CE to  $r = 0.65$  from 1,226 to 1,500 as a function of reduced site and sample replication (Figure S2). The decay in network coherence back in time, due to changing numbers of trees, is characteristic for millennial-length climate reconstructions (Esper *et al.*, 2016; Ljungqvist *et al.*, 2020) and here estimated by adding bootstrap confidence limits, derived from resampling the TRW data, to the final reconstruction (see below).

The 500-year spline detrended PNP site chronologies correlate reasonably well against regional June–July precipitation data over the past 40 years ranging from  $r = 0.26$  in Val2 to  $r = 0.76$  in Smo4 (Figure 4). The exceptionally low value in Val2 is likely related to the reduced sample replication at this site integrating TRW data from only 10 trees, though other low-replicated sites from the Mt. Smolikas massif correlate better (Smo9, 10 and 12 at  $r = 0.50$ – $0.68$ ; Table S1). The overall weaker precipitation signal in the Val pine sites is also reflected in the mean chronologies ( $r_{\text{Val}} = 0.60$  and  $r_{\text{Smo}} = 0.74$  from 1976 to 2015), but this difference is statistically insignificant. Besides these regional differences, systematically lower correlations are found when extending the calibration period stepwise back over the 20th century (bottom panel of Figure 4). The correlation decline is seen in all site chronologies and likely reflects a deterioration of the CRU TS 4.04 gridded precipitation data as fewer (and more remote) instrumental station records are included in the calibration target back in time (Klippel *et al.*, 2018). An additionally contributing temperature influence is not retained in the HEPI TRW data as the monthly and seasonal correlations reveal no significant results over various periods since 1901 (Figure S3).

The TRW mean, combining all PNP site chronologies, correlates at  $r_{1976-2015} = 0.71$  ( $p < .001$ ) with June–July precipitation indicating that about half of the instrumental data variance can be explained by the proxy network. Considering no instrumental station data representative of the moist conditions found at the PNP treeline sites



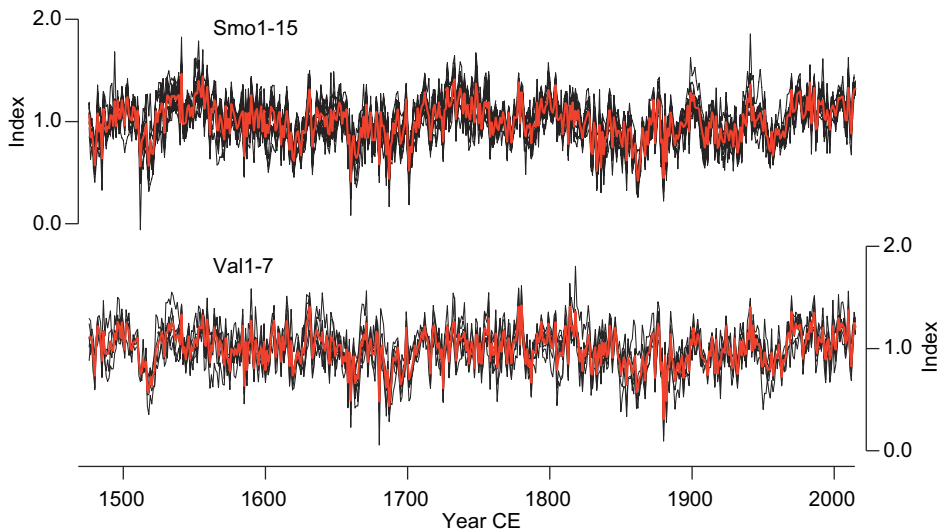


**FIGURE 3** 500-year spline detrended *Pinus heldreichii* site chronologies (black curves) from the Mt. Smolikas (top) and Valia Calda regions (bottom) and their means (red curves) since 1,476 CE [Colour figure can be viewed at [wileyonlinelibrary.com](http://wileyonlinelibrary.com)]

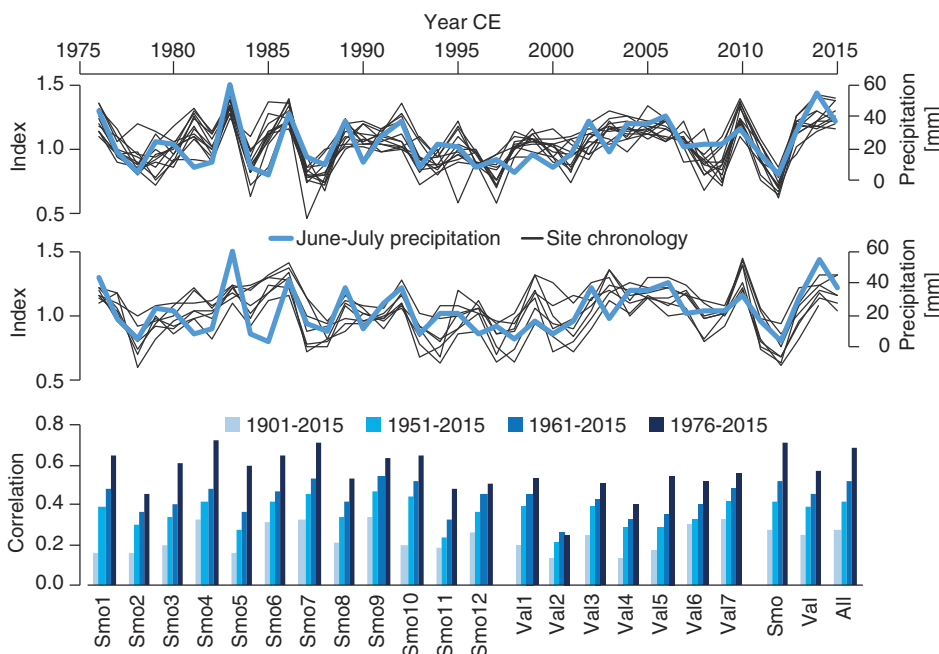


**FIGURE 4** Calibration of the Mt. Smolikas (top panel) and Valia Calda (middle panel) site chronologies in black against CRU TS 4.04 average June–July precipitation in blue from 1976 to 2015. Bottom panel shows the correlations of the single sites chronologies, as well as the mean of the Smolikas sites (Smo), Valia Calda sites (Val) and all sites (All), over the 1901–2015, 1951–2015, 1961–2015 and 1976–2015 periods [Colour figure can be viewed at [wileyonlinelibrary.com](http://wileyonlinelibrary.com)]

were available, this measure of signal strength is at best a conservative estimate. The precipitation signal also weakens when more flexible splines are used for detrending, that is, less low-frequency variance is retained in the resulting TRW chronologies, from  $r = 0.71$  in the 500-year spline detrended HEPI chronology, to  $r_{300spl} = 0.69$  and  $r_{100spl} = 0.66$  (but  $r_{50spl} = 0.68$ ) in the more rigorously detrended chronologies. This conclusion is supported by additional tests using first-differenced proxy and instrumental data revealing a correlation decline from  $r_{500spl} = 0.71$  to  $r_{FirstDiff} = 0.64$  over the 1976–2015 period.

Reviewing the calibration results commensurate with the various detrending options, suggests some of the low-frequency TRW variance retained over the relatively

short calibration period of only 40 years contains hydro-climatic information. However, the correlations of the first-differenced instrumental and proxy data are slightly higher over the extended 1961–2015 ( $r_{FirstDiff} = 0.62$  compared to  $r_{500spl} = 0.51$ ), 1951–2015 ( $r_{FirstDiff} = 0.57$ ,  $r_{500spl} = 0.41$ ), and 1901–2015 periods ( $r_{FirstDiff} = 0.31$ ,  $r_{500spl} = 0.24$ ). These values indicate that the low-frequency variance in the instrumental data during the mid and early 20th century is not well reflected in the 500-year spline detrended HEPI chronology, suggesting that such variability in the millennial-length reconstruction should cautiously be interpreted. On the other hand, as no instrumental station record is available representing the moist high-elevation PNP conditions, and since even fewer and more remote station records are

combined during the mid and early 20th century, this lack of reliable observations signifies that small correlation changes against early CRU TS data should not be overinterpreted. In contrast, the highly synchronous 500-year spline detrended TRW site chronologies, across the PNP and over centuries (Figure 3), demonstrate that a formal precipitation reconstruction retaining high-to-low frequency variance can be developed using the HEPI network. This conclusion is supported by the lack of correlation between the HEPI TRW chronology and a millennial-length temperature reconstruction based on maximum latewood densities from Mt. Smolikas Bosnian pines (Esper *et al.*, 2020). The density-based reconstruction correlates at 0.73 against instrumental temperatures and shows dissimilar high-to-low frequency variance over the past 12 centuries compared to the new precipitation record (Figure S4).

### 3.2 | June–July precipitation reconstruction and benchmarking

The regressed 500-year spline detrended HEPI chronology from northwestern Greece shows ample high-to-low frequency June–July precipitation variance over the past 1,278 years (Figure 5). The reconstruction is characterized by increasing uncertainties back in time, expressed by the expanding bootstrap confidence range (the red curves in Figure 5(a)), which is largely a function of the reduced sample replication and changing interseries correlation over the past 13 centuries (Figure 5(c–d)). The

EPS metric exceeds the widely considered 0.85 threshold back to 755 CE indicating that the samples integrated in the reconstruction represent to some degree the infinite population (Wigley *et al.*, 1984). Split-period correlation ( $r_{1976-1995} = 0.69$ ,  $r_{1996-2015} = 0.74$ ), RE (0.47–0.81), CE (0.47–0.53) and DW statistics (1.83) demonstrate a reasonable and temporally stable fit with instrumental June–July precipitation data, reinforcing the skill of the TRW-based reconstruction. Caution is needed, however, as much of the reconstructed inter-annual to centennial scale variance occurs outside the range of variance captured by the relatively short instrumental station data (the blue curve in Figure 5(a); von Storch *et al.*, 2004). This is particularly the case during the exceptionally dry periods and extremes reconstructed over the past 13 centuries displaying values well below the mean of the adjusted instrumental data (73 mm from 1976 to 2015). This basic uncertainty applies to many climate reconstructions (Büntgen *et al.*, 2011; Klesse *et al.* 2015) particularly those that place the current warm conditions in a long-term context (Esper *et al.*, 2002, 2014, 2018; D'Arrigo *et al.*, 2006; Juckes *et al.*, 2007; Ljungqvist, 2010; Pages 2 K Consortium, 2013; Schneider *et al.*, 2015; Luterbacher *et al.*, 2016; Wilson *et al.*, 2016; Anchukaitis *et al.*, 2017).

The new reconstruction shows substantial decadal-to-centennial scale precipitation variability including a long-term increase from dry conditions in the mid-19th century ( $1,846-1,875 = 42 \pm 2.3$  mm) towards recent pluvial conditions ( $1986-2015 = 73 \pm 2$  mm; Table S2). The driest reconstructed 30-year periods occurred from 1,350–1,379 CE ( $39 \pm 4.5$  mm) and 913–942

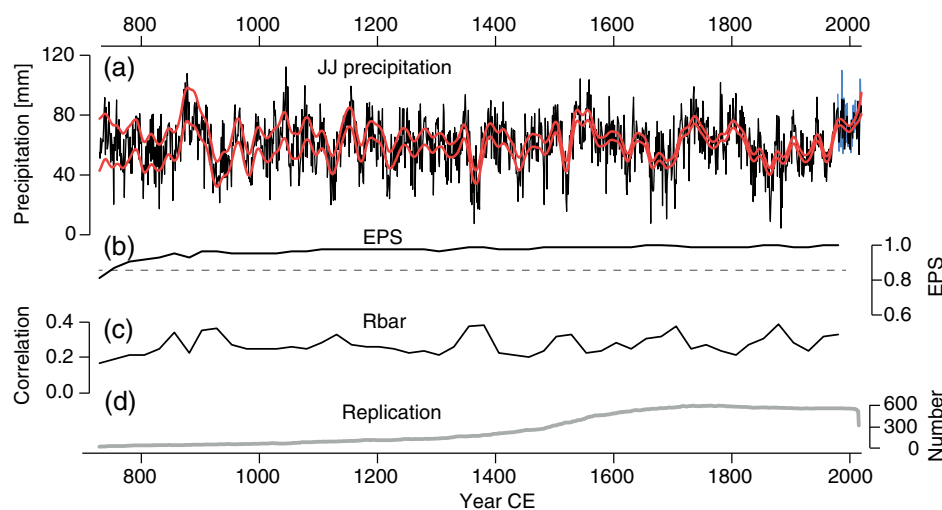


**FIGURE 5** Precipitation reconstruction and characteristics. (a) June–July precipitation reconstruction (black curve) derived from regressing the 500-year spline detrended HEPI chronology against adjusted instrumental data (blue curve). Red curves are 30-year smoothed 95% bootstrap confidence intervals from re-sampling and averaging the detrended series with replacement 1,000 times. (b) The expressed population signal, (c) Rbar, and (d) sample replication curves of the HEPI chronology back to 729 CE [Colour figure can be viewed at [wileyonlinelibrary.com](https://onlinelibrary.wiley.com)]

( $40 \pm 8.4$  mm), although the estimated uncertainties increase back in time as a function of reduced TRW sample replication. The most pluvial periods are 862–891 CE ( $86 \pm 11$  mm) and 1,539–1,568 ( $80 \pm 3.4$  mm) during which the precipitation estimates exceeded the dry period values by  $>40$  mm. These long-term changes are accompanied by numerous extreme events including the exceptionally dry early summers in 1,362, 1,660, 1,880 and 1,862 CE when precipitation was  $<10$  mm, and the exceptionally moist early summers in 877, 1,044, 1,541 and 1,556 CE when precipitation was  $>100$  mm. The overall variability of reconstructed June–July precipitation over the past 13 centuries thereby exceeds 90 mm at the inter-annual timescale, and could even be  $>100$  mm if the bootstrap-derived reconstruction confidence interval is considered (Table S2).

The character of the reconstruction presented here depends on the detrending method used to produce the HEPI mean chronology and the technique applied to transform this chronology into estimates of June–July precipitation. The reconstructed variability is a function of the unexplained variance of the regression between TRW and instrumental data. The transfer method (e.g., regression or scaling), and to some degree the period of overlap with instrumental data (here 40 years from 1976–2015), are operator choices, and changing these alters the reconstruction variance (Esper *et al.*, 2005). Additional uncertainty arises from the choice of detrending method, as the 500-year spline detrended chronology used here for reconstruction preserves systematically more low-frequency variance, and thus more precipitation variability over the past 13 centuries, compared to the 300-, 100- and 50-year chronologies (Figure S5). Finally, the adjustment applied to the instrumental precipitation data affects the range of reconstructed values. If the 500-year spline detrended HEPI chronology is regressed against unadjusted CRU precipitation data, negative reconstructed values (down to  $-40$  mm) appear throughout the past 1,278 years (bottom panel in Figure S5(a)). This problem applies to all chronologies including those that are limited in preserving low-frequency variance (top panels in Figure S5(a)), demonstrating that any reconstruction effort is affected if the scale of instrumental data is not sufficiently representative of the climate conditions where trees grow.

Our new reconstruction presented here contains substantially more low-frequency variance compared to the June–July SPI reconstruction from northwestern Greece (Klippel *et al.*, 2018), the May–June precipitation reconstruction extending into northeastern Turkey (Griggs *et al.*, 2007), and the May–August precipitation reconstruction based on multiple tree sites in Turkey, Syria, Lebanon, Cyprus and Greece (Touchan *et al.*, 2005;

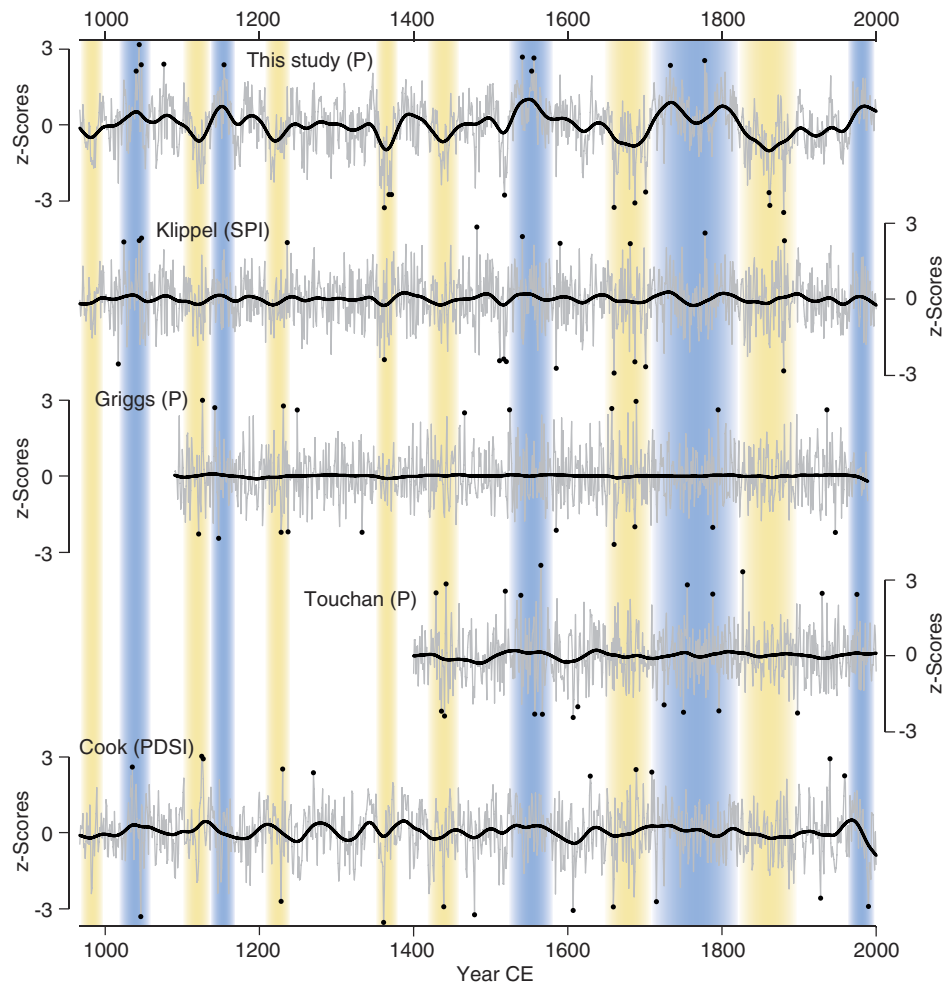
Figure 6). This spectral difference (Figure S7) is likely unrelated to differences in season or spatial coverage but traces back to the different detrending methods applied to the reconstructions including more flexible high-pass filtering techniques used in the previous attempts. While we do not contest this approach and have ourselves used cubic smoothing splines and pre-whitening techniques in the study by Klippel *et al.* (2018) to avoid introducing any lower-frequency variance that is not related to hydroclimate, the current network analysis and coherence among 22 *Pinus heldreichii* sites enabled us to overcome this constraint and preserve more low-frequency variance in the final reconstruction. As a consequence, the periods of multi-decadal dry and moist summers highlighted in yellow and blue in Figure 6 are not captured by the three other SPI and precipitation reconstructions from the eastern Mediterranean.

The situation is different with the PDSI reconstruction derived from regional grid points of the Old World drought atlas (bottom panel in Figure 6; Cook *et al.*, 2015). This record contains substantially more low-frequency variance than the SPI and precipitation records, albeit not as much as the HEPI-based reconstruction presented here (Figure S7). There is little coherence between the June–August PDSI and the new June–July precipitation reconstructions over the past millennium, and the discrepancies are perhaps greatest during the most recent decades when the PDSI record indicates a sharp trend towards drier conditions, whereas the new precipitation record indicates moist conditions. These contradictions are likely related to the varying hydroclimatic targets (PDSI vs. precipitation) and the methods used to combine data in the drought atlas. The tree-ring chronologies used to produce the drought atlas were detrended to retain centennial to multi-centennial variance (using RCS and Signal Free; Esper *et al.*, 2003; Melvin and Briffa, 2008), but their combination can include a reversal of chronology values if regional drought is controlled by longer-term temperature increases rather than precipitation shortages, as is the case in most Mediterranean regions since the mid-20th century. Consequently, we argue that late 20th century downward trend in reconstructed PDSI reflects an increase in drought severity driven by rising temperatures. It is therefore understandable why an equivalent negative trend is not seen in the high-elevation precipitation reconstruction presented here.

Beyond low-frequency variance, there is minor to almost no coherence among the extreme events recorded in the high-resolution hydroclimate reconstructions from the northwestern Mediterranean (the black dots in Figure 6). Whereas the precipitation reconstructions correlate between  $r = 0.17$  and  $r = 0.32$  from 1,400 to



**FIGURE 6** Comparison of the PNP precipitation reconstruction (this study) with a high-frequency SPI reconstruction from Mt. Smolikas trees (Klippel), a May–June precipitation reconstruction from oak trees in northwestern Greece and northeastern Turkey (Griggs), a May–August precipitation reconstruction from tree sites in Turkey, Syria, Lebanon, Cyprus and Greece (Touchan), and a June–August PDSI reconstruction from grid points in northeastern Greece (Cook). All records were z-scored over the common 1400–2000 period. Black curves are 50-year splines, and black dots indicate the 10 wettest and driest extremes over the past 600 to 1,000 years. Yellow and blue bars indicate dry and wet periods, during which the 50-year spline of PNP reconstruction exceeds 1 *SD* [Colour figure can be viewed at [wileyonlinelibrary.com](http://wileyonlinelibrary.com)]



2,000 CE (Table S3), only 2 of the 10 driest and wettest summers retained in the HEPI network concur with the Griggs *et al.* (2007) record (Table S2;  $1,660 = 8 \pm 2.5$  mm,  $1,687 = 11 \pm 2.4$  mm), and none with Touchan *et al.* (2005). This lack of high-frequency coherency is consistent with the nature of regional summer rainfall that is typically driven by local depressions and spatially constrained convection and thunderstorms. These rain-laden events are not expected to align between records integrating data from different countries in the eastern Mediterranean and even less likely to agree with remote records from Turkey (Akkemik and Aras, 2005; Touchan *et al.*, 2007; Köse *et al.*, 2013), France (Szymczak *et al.*, 2014), Spain (Esper *et al.*, 2015a; Tejedor *et al.*, 2016, 2017, 2019), Morocco (Esper *et al.*, 2007), or Tunisia (Touchan *et al.*, 2008).

## 4 | CONCLUSIONS

A June–July precipitation reconstruction extending back to 729 CE is presented for northwestern Greece. The record is derived from a network of 22 high-elevation

pine sites revealing highly coherent growth variations over the past centuries across the Pindus Mountains. Particular emphasis is placed on retaining low-frequency, multi-decadal precipitation variability retained in this network in order to illustrate how conditions since the late 20th century are comparatively moist relative to the range of likely precipitation fluctuations over the past millennium. This conclusion refers to precipitation variability only, that is, does not consider the warming trend recorded since the late 20th century (Rohde *et al.*, 2013) nor the temperature changes during pre-instrumental times (Esper *et al.*, 2020). A distinct differentiation between precipitation and temperature reconstructions is feasible in northwestern Greece as the TRW and maximum latewood density data from the same high-elevation pines do not correlate so that independent assessments of natural hydroclimate and temperature variability could be developed (Klippel *et al.*, 2018; Esper *et al.*, 2020).

The comparison with other statistically calibrated hydroclimate reconstructions from the eastern Mediterranean revealed little coherence over the past 600–1,000 years (Touchan *et al.*, 2005; Griggs *et al.*, 2007). This conclusion is likely driven by the (a) spatially

heterogeneous precipitation patterns, particularly during the summer months when local thunderstorms feed the aquifers in high-elevation environments, and (b) different detrending methods applied to the varying reconstructions limiting their ability to retain low-frequency hydroclimate variations over the past centuries. Whereas the lack of coherence with existing records does not necessarily support the conclusions presented here, it appears hard to imagine that other factors, beyond precipitation, affected tree growth and synchronized TRW chronologies over centuries among multiple sites in the Pindus Mountains. An alternative driver could be CO<sub>2</sub>, although the muted pre-industrial atmospheric variations, <10 ppm at inter-decadal timescales (Frank *et al.*, 2010), cannot explain the highly synchronous pre-Anthropocene (Foley *et al.*, 2013) growth variations reported here. The development of further high-resolution reconstructions emphasizing low-frequency hydroclimate variability over the past centuries to millennia would be key to place the current dynamics into a long-term context. An improved understanding of pre-instrumental, natural hydroclimate variability is particularly needed for the Mediterranean region that is threatened by substantial drying over the upcoming decades.

## ACKNOWLEDGEMENTS

The authors thank Robert Brandes for pointing towards old-growth forest sites in Greece, and Yannik Esser, Markus Kochbeck, Eileen Kuhl, Philipp Römer, Marcel Wilhelm and Birgit Wöste for TRW measurements. Supported by the German Science Foundation project ES 161/12-1. Open access funding enabled and organized by Projekt DEAL.

## ORCID

Jan Esper  <https://orcid.org/0000-0003-3919-014X>

Lara Klippel  <https://orcid.org/0000-0003-3032-7920>

## REFERENCES

- Akkemik, Ü. and Aras, A. (2005) Reconstruction (1689–1994 AD) of April–August precipitation in the southern part of Central Turkey. *International Journal of Climatology*, 25, 537–548.
- Anchukaitis, K.J., Wilson, R., Briffa, K.R., Büntgen, U., Cook, E.R., D'Arrigo, R., Davi, N., Esper, J., Frank, D., Gunnarson, B.E., Hegerl, G., Helama, S., Klesse, S., Krusic, P.J., Linderholm, H. W., Myglan, V., Osborn, T.J., Zhang, P., Rydval, M., Schneider, L., Schurer, A., Wiles, G. and Zorita, E. (2017) Last millennium northern hemisphere summer temperatures from tree rings: part II, spatially resolved reconstructions. *Quaternary Science Reviews*, 163, 1–22.
- Briffa, K.R., Jones, P.D., Bartholin, T.S., Eckstein, D., Schweingruber, F.H., Karlen, W., Zetterberg, P. and Eronen, M. (1992) Fennoscandian summers from AD 500: temperature changes on short and long timescales. *Climate Dynamics*, 7, 111–119.
- Büntgen, U., Tegel, W., Nicolussi, K., McCormick, M., Frank, D., Trouet, V., Kaplan, J.O., Herzig, F., Heussner, K.U., Wanner, H., Luterbacher, J. and Esper, J. (2011) 2500 years of European climate variability and human susceptibility. *Science*, 331, 578–582.
- Cook, E.R. and Peters, K. (1981) The smoothing spline: a new approach to standardizing forest interior tree-ring width series for dendroclimatic studies. *Tree-Ring Bulletin*, 41, 45–53.
- Cook, E.R. and Kairiukstis, L.A. (1990) *Methods of Dendrochronology – Applications in the Environmental Science*. Dordrecht, the Netherlands: Kluwer.
- Cook, E.R., Briffa, K.R. and Jones, P.D. (1994) Spatial regression methods in dendroclimatology: a review and comparison of two techniques. *International Journal of Climatology*, 14, 379–402.
- Cook, E.R. and Peters, K. (1997) Calculating unbiased tree-ring indices for the study of climatic and environmental change. *The Holocene*, 7, 361–370.
- Cook, E.R., Seager, R., Kushnir, Y., Briffa, K.R., Büntgen, U., Frank, D., Krusic, P.J., Tegel, W., van der Schrier, G., Andreu-Hayles, L., Baillie, M., Baittinger, C., Bleicher, N., Bonde, N., Brown, D., Carrer, M., Cooper, R., Čufar, K., Dittmar, C., Esper, J., Griggs, C., Gunnarson, B., Günther, B., Gutierrez, E., Haneca, K., Helama, S., Herzig, F., Heussner, K.U., Hofmann, J., Janda, P., Kontic, R., Köse, N., Kyncl, T., Levanič, T., Linderholm, H., Manning, S., Melvin, T.M., Miles, D., Neuwirth, B., Nicolussi, K., Nola, P., Panayotov, M., Popa, I., Rothe, A., Seftigen, K., Seim, A., Svarva, H., Svoboda, M., Thun, T., Timonen, M., Touchan, R., Trotsiuk, V., Trouet, V., Walder, F., Ważny, T., Wilson, R. and Zang, C. (2015) Old World megadroughts and pluvials during the common era. *Science Advances*, 1, e1500561.
- Cook, E.R., Krusic, P.J., Peters, K. and Holmes, R.L. (2017) Program ARSTAN (version 49v1a) autoregressive tree-ring standardization program. Tree-Ring Laboratory of Lamont–Doherty Earth Observatory. Available at: <http://www.ldeo.columbia.edu/tree-ring-laboratory/resources/software>
- D'Arrigo, R., Wilson, R. and Jacoby, G. (2006) On the long-term context for late twentieth century warming. *Journal of Geophysical Research*, 111(D3).
- Durbin, J. and Watson, G.S. (1951) Testing for serial correlation in least squares regression. II. *Biometrika*, 38, 159–178.
- Esper, J., Cook, E.R. and Schweingruber, F.H. (2002) Low-frequency signals in long tree-ring chronologies and the reconstruction of past temperature variability. *Science*, 295, 2250–2253.
- Esper, J., Cook, E.R., Krusic, P.J., Peters, K. and Schweingruber, F. H. (2003) Tests of the RCS method for preserving low-frequency variability in long tree-ring chronologies. *Tree-Ring Research*, 59, 81–98.
- Esper, J., Frank, D.C., Wilson, R.J. and Briffa, K.R. (2005) Effect of scaling and regression on reconstructed temperature amplitude for the past millennium. *Geophysical Research Letters*, 33, 7.
- Esper, J., Frank, D., Büntgen, U., Verstege, A., Luterbacher, J. and Xoplaki, E. (2007) Long-term drought severity variations in Morocco. *Geophysical Research Letters*, 34(17).
- Esper, J., Duthorn, E., Krusic, P., Timonen, M. and Büntgen, U. (2014) Northern European summer temperature variations over

- the common era from integrated tree-ring density records. *Journal of Quaternary Science*, 29, 487–494.
- Esper, J., Großjean, J., Camarero, J.J., García-Cervigón, A.I., Olano, J.M., González-Rouco, J.F., Domínguez-Castro, F. and Büntgen, U. (2015a) Atlantic and Mediterranean synoptic drivers of central Spanish juniper growth. *Theoretical and Applied Climatology*, 121, 571–579.
- Esper, J., Schneider, L., Smerdon, J.E., Schöne, B.R. and Büntgen, U. (2015b) Signals and memory in tree-ring width and density data. *Dendrochronologia*, 35, 62–70.
- Esper, J., Krusic, P.J., Ljungqvist, F.C., Luterbacher, J., Carrer, M., Cook, E., Davi, N.K., Hartl-Meier, C., Kirilyanov, A., Konter, O., Myglan, V., Timonen, M., Treyde, K., Trouet, V., Villalba, R., Yang, B. and Büntgen, U. (2016) Ranking of tree-ring based temperature reconstructions of the past millennium. *Quaternary Science Reviews*, 145, 134–151.
- Esper, J., George, S.S., Anchukaitis, K., D'Arrigo, R., Ljungqvist, F.C., Luterbacher, J., Schneider, L., Stoffel, M., Wilson, R. and Büntgen, U. (2018) Large-scale, millennial-length temperature reconstructions from tree-rings. *Dendrochronologia*, 50, 81–90.
- Esper, J., Klippel, L., Krusic, P.J., Konter, O., Raible, C.C., Xoplaki, E., Luterbacher, J. and Büntgen, U. (2020) Eastern Mediterranean summer temperatures since 730 CE from Mt. Smolikas tree-ring densities. *Climate Dynamics*, 54, 1367–1382.
- Frank, D.C., Esper, J., Raible, C.C., Büntgen, U., Trouet, V., Stocker, B. and Joos, F. (2010) Ensemble reconstruction constraints on the global carbon cycle sensitivity to climate. *Nature*, 463, 527–530.
- Foley, S.F., Gronenborn, D., Andreae, M.O., Kadereit, J.W., Esper, J., Scholz, D., Pöschl, U., Jacob, D.E., Schöne, B.R., Schreg, R., Vött, A., Jordan, D., Lelieveld, J., Weller, C.G., Alt, K.W., Gaudzinski-Windheuser, S., Bruhn, K.C., Tost, H., Sirocko, F. and Crutzen, P.J. (2013) The Palaeoanthropocene – the beginnings of anthropogenic environmental change. *Anthropocene*, 3, 83–88.
- Fotiadi, A.K., Metaxas, D.A. and Bartzoka, A. (1999) A statistical study of precipitation in northwestern Greece. *International Journal of Climatology*, 19, 1221–1232.
- Frank, D., Esper, J. and Cook, E.R. (2007) Adjustment for proxy number and coherence in a large-scale temperature reconstruction. *Geophysical Research Letters*, 34(16).
- Fritts, H. (1976) *Tree Rings and Climate*. London, UK: Academic Press.
- Griggs, C., DeGaetano, A., Kuniholm, P. and Newton, M. (2007) A regional high-frequency reconstruction of May–June precipitation in the north Aegean from oak tree rings, AD 1089–1989. *International Journal of Climatology*, 27, 1075–1089.
- Harris, I., Jones, P.D., Osborn, T.J. and Lister, D.H. (2014) Updated high-resolution grids of monthly climatic observations – the CRU TS3.10 dataset. *International Journal Climatology*, 34, 623–642.
- Hatzianastassiou, N., Katsoulis, B., Pnevmatikos, J. and Antakis, V. (2008) Spatial and temporal variation of precipitation in Greece and surrounding regions based on global precipitation climatology project data. *Journal of Climate*, 21, 1349–1370.
- Juckes, M.N., Allen, M.R., Briffa, K.R., Esper, J., Hegerl, G.C., Moberg, A., Osborn, T.J. and Weber, S.L. (2007) Millennial temperature reconstruction intercomparison and evaluation. *Climate of the Past*, 3, 591–609.
- Klesse, S., Ziehmer, M., Rousakis, G., Trouet, V. and Frank, D. (2015) Synoptic drivers of 400 years of summer temperature and precipitation variability on Mt. Olympus, Greece. *Climate Dynamics*, 45, 807–824.
- Klippel, L., Krusic, P.J., Brandes, R., Hartl-Meier, C., Trouet, V., Meko, M. and Esper, J. (2017) High-elevation inter-site differences in Mount Smolikas tree-ring width data. *Dendrochronologia*, 44, 164–173.
- Klippel, L., Krusic, P.J., Brandes, R., Hartl, C., Belmecheri, S., Dienst, M. and Esper, J. (2018) A 1286-year hydro-climate reconstruction for the Balkan Peninsula. *Boreas*, 47, 1218–1229.
- Klippel, L., Krusic, P.J., Konter, O., St. George, S., Trouet, V. and Esper, J. (2019) A 1200+ year reconstruction of temperature extremes for the northeastern Mediterranean region. *International Journal of Climatology*, 39, 2336–2350.
- Köse, N., Akkemik, Ü., Güner, H.T., Dalfes, H.N., Grissino-Mayer, H.D., Özeren, M.S. and Kindap, T. (2013) An improved reconstruction of May–June precipitation using tree-ring data from western Turkey and its links to volcanic eruptions. *International Journal of Biometeorology*, 57, 691–701.
- Konter, O., Krusic, P.J., Trouet, V. and Esper, J. (2017) Meet Adonis, Europe's oldest dendrochronologically dated tree. *Dendrochronologia*, 42, 12.
- Li, W., Li, L., Ting, M. and Liu, Y. (2012) Intensification of northern hemisphere subtropical highs in a warming climate. *Nature Geoscience*, 5, 830–834.
- Ljungqvist, F.C. (2010) A new reconstruction of temperature variability in the extra-tropical northern hemisphere during the last two millennia. *Geografiska Annaler*, 92, 339–351.
- Ljungqvist, F.C., Piermattei, A., Seim, A., Krusic, P.J., Büntgen, U., He, M., Kirilyanov, A.V., Luterbacher, J., Schneider, L., Seftigen, K., Stahle, D.W., Villalba, R., Yang, B. and Esper, J. (2020) Ranking of tree-ring based hydroclimate reconstructions of the past millennium. *Quaternary Science Reviews*, 230, 106074.
- Luterbacher, J., Werner, J.P., Smerdon, J.E., Fernández-Donado, L., González-Rouco, F.J., Barriopedro, D., Ljungqvist, F.C., Büntgen, U., Zorita, E., Wagner, S., Esper, J., McCarroll, D., Toreti, A., Frank, D., Jungclaus, J.H., Barriendos, M., Bertolin, C., Bothe, O., Brázdil, R., Camuffo, D., Dobrovolný, P., Gagen, M., García-Bustamante, E., Ge, Q., Gómez-Navarro, J.J., Guiot, J., Hao, Z., Hegerl, G.C., Holmgren, K., Klimenko, V.V., Martín-Chivelet, J., Pfister, C., Roberts, N., Schindler, A., Schurer, A., Solomina, O., von Gunten, L., Wahl, E., Wanner, H., Wetter, O., Xoplaki, E., Yuan, N., Zanchettin, D., Zhang, H. and Zerefos, C. (2016) European summer temperatures since Roman times. *Environmental Research Letters*, 11, 024001.
- Meko, D., Cook, E.R., Stahle, D.W., Stockton, C.W. and Hughes, M. K. (1993) Spatial patterns of tree-growth anomalies in the United States and southeastern Canada. *Journal of Climate*, 6, 1773–1786.
- Melvin, T.M. and Briffa, K.R. (2008) A “signal-free” approach to dendroclimatic standardisation. *Dendrochronologia*, 26, 71–86.
- Osborn, T.J., Briffa, K.R. and Jones, P.D. (1997) Adjusting variance for sample-size in tree-ring chronologies and other regional-mean time-series. *Dendrochronologia*, 15, 89–99.
- PAGES 2k Consortium. (2013) Continental-scale temperature variability during the past two millennia. *Nature Geoscience*, 6, 339–346.
- Rohde, R., Muller, R., Jacobsen, R., Perlmuter, S., Rosenfeld, A., Wurtele, J., Curry, J., Wickham, C. and Mosher, S. (2013) A new estimate of the average earth surface land temperature

- spanning 1753 to 2011. *Geoinformatics Geostatistics: An Overview*, 1, 1. <https://doi.org/10.4172/2327-4581.1000101>.
- Schneider, L., Smerdon, J., Büntgen, U., Wilson, R., Myglan, V.S., Kirdyanov, A. and Esper, J. (2015) Revising midlatitude summer temperatures back to AD 600 based on a wood density network. *Geophysical Research Letters*, 42, 4556–4562.
- Szymczak, S., Hetzer, T., Bräuning, A., Joachimski, M.M., Leuschner, H.H. and Kuhlemann, J. (2014) Combining wood anatomy and stable isotope variations in a 600-year multiparameter climate reconstruction from Corsican black pine. *Quaternary Science Reviews*, 101, 146–158.
- Tejedor, E., de Luis, M., Cuadrat, J.M., Esper, J. and Saz, M.Á. (2016) Tree-ring-based drought reconstruction in the Iberian range (east of Spain) since 1694. *International Journal of Biometeorology*, 60, 361–372.
- Tejedor, E., Saz, M.A., Esper, J., Cuadrat, J.M. and de Luis, M. (2017) Summer drought reconstruction in northeastern Spain inferred from a tree ring latewood network since 1734. *Geophysical Research Letters*, 44, 8492–8500.
- Tejedor, E., De Luis, M., Barriendos, M., Cuadrat, J.M., Luterbacher, J. and Saz, M.Á. (2019) Rogation ceremonies: a key to understanding past drought variability in northeastern Spain since 1650. *Climate of the Past*, 15, 1647–1664.
- Touchan, R., Xoplaki, E., Funkhouser, G., Luterbacher, J., Hughes, M.K., Erkan, N., Akkemik, Ü. and Stephan, J. (2005) Reconstructions of spring/summer precipitation for the Eastern Mediterranean from tree-ring widths and its connection to large-scale atmospheric circulation. *Climate Dynamics*, 25, 75–98.
- Touchan, R., Akkemik, Ü., Hughes, M.K. and Erkan, N. (2007) May–June precipitation reconstruction of southwestern Anatolia, Turkey during the last 900 years from tree rings. *Quaternary Research*, 68, 196–202.
- Touchan, R., Meko, D.M. and Aloui, A. (2008) Precipitation reconstruction for northwestern Tunisia from tree rings. *Journal of Arid Environments*, 72, 1887–1896.
- Trouet, V. and Van Oldenborgh, G.J. (2013) KNMI climate explorer: a web-based research tool for high-resolution paleoclimatology. *Tree-Ring Research*, 69, 3–13.
- van der Schrier, G., Barichivich, J., Briffa, K.R. and Jones, P.D. (2013) A scPDSI-based global data set of dry and wet spells for 1901–2009. *Journal of Geophysical Research: Atmospheres*, 118, 4025–4048.
- Von Storch, H., Zorita, E., Jones, J.M., Dimitriev, Y., González-Rouco, F. and Tett, S.F. (2004) Reconstructing past climate from noisy data. *Science*, 306, 679–682.
- Wigley, T.M., Briffa, K.R. and Jones, P.D. (1984) On the average value of correlated time series, with applications in dendroclimatology and hydrometeorology. *Journal of Climate and Applied Meteorology*, 23, 201–213.
- Wilson, R., Anchukaitis, K., Briffa, K.R., Büntgen, U., Cook, E., D'Arrigo, R., Davi, N., Esper, J., Frank, D., Gunnarson, B., Hegerl, G., Helama, S., Klesse, S., Krusic, P.J., Linderholm, H.W., Myglan, V., Osborn, T.J., Rydval, M., Schneider, L., Schurer, A., Wiles, G., Zhang, P. and Zorita, E. (2016) Last millennium Northern hemisphere summer temperatures from tree rings. Part I: the long term context. *Quaternary Science Reviews*, 134, 1–18.
- Zhang, H. and Oweis, T. (1999) Water–yield relations and optimal irrigation scheduling of wheat in the Mediterranean region. *Agricultural Water Management*, 38, 195–211.

## SUPPORTING INFORMATION

Additional supporting information may be found online in the Supporting Information section at the end of this article.

**How to cite this article:** Esper J, Konter O, Klippel L, Krusic PJ, Büntgen U. Pre-instrumental summer precipitation variability in northwestern Greece from a high-elevation *Pinus heldreichii* network. *Int J Climatol*. 2021;1–12. <https://doi.org/10.1002/joc.6992>